Compton scattering of polarized γ rays by ^{16}O for E_γ=25–40 MeV

B. A. Perdue, M. W. Ahmed, A. P. Tonchev, and H. R. Weller
Triangle Universities Nuclear Laboratory, Duke University, P.O. Box 90308, Durham, North Carolina 27708, USA

G. Feldman
Department of Physics, George Washington University, Washington, D.C. 20052, USA

V. N. Litvinenko and I. V. Pinayev
Duke Free Electron Laser Laboratory, Duke University, P.O. Box 90319, Durham, North Carolina 27708, USA

B. E. Norum
Department of Physics, University of Virginia, P.O. Box 400714, Charlottesville, Virginia 22903, USA

R. M. Prior and M. C. Spraker
North Georgia College & State University, Dahlonega, Georgia 30597, USA

B. D. Sawatzky
Department of Physics, University of Virginia, P.O. Box 400714, Charlottesville, Virginia 22904, USA
(Received 2 July 2004; published 9 December 2004)

Measurements of the polarization asymmetries $\Sigma(\theta_{\mathrm{c.m.}})$ and $\Sigma(E_\gamma)$ of Compton scattering by ^{16}O have been performed in the energy range of 25–40 MeV over a range of scattering angles between 90 and 150°. An analysis of the present data combined with previous results indicates that significant, narrow concentrations of $E2$ strength are not present below an excitation energy of 40 MeV. The existence, however, of a broad isovector giant quadrupole resonance exhausting a large percentage of the isovector energy weighted sum rule is not ruled out by the combined data. Additionally, the present data are insensitive to modifications to the free values of the nucleon polarizabilities, but cannot rule them out.

DOI: 10.1103/PhysRevC.70.064305 PACS number(s): 24.30.Cz

I. INTRODUCTION

A. Motivation

It has been demonstrated for Compton scattering of polarized photons from ^{208}Pb [1] that an isovector giant quadrupole resonance (IVGQR) signature can be seen in the ratio of differential cross sections $(d\sigma/d\Omega)_\perp/(d\sigma/d\Omega)_\parallel$. The $\perp$ and $\parallel$ subscripts indicate the perpendicular and parallel components of the cross section, respectively. The main goal of the present experiment was to determine experimental parameters for the IVGQR in ^{16}O below E_γ=40 MeV. A secondary goal was to explore the sensitivity of the present data to medium modifications of the free values of the proton-neutron averaged electromagnetic nucleon polarizabilities.

The secondary goal arose because there are inconsistencies between previous results on ^{16}O [2–5], and our intent was to use the data taken in the present experiment to reconcile the inconsistencies. From data obtained at Lund [2], Hütt *et al.* [3] conclude that in-medium polarizabilities "are the same as the corresponding quantities for the free nucleon within a precision of order of $\pm 2.5\times 10^{-4}$ fm^3." On the other hand, Feldman *et al.* find that "either a substantial modification of the nucleon polarizabilities or a significant energy dependence to the [two-body portion of the scattering amplitude] is required" to represent data taken at the Saskatchewan Accelerator Laboratory (SAL) [4] and the University of Illinois [5]. The discrepancy is due strictly to a disagreement in the measured cross sections at large angles.

B. Previous studies of GQRs in ^{16}O

Although extensively studied, the parameters of both the isoscalar giant quadrupole resonance (ISGQR) and the isovector giant quadrupole resonance (IVGQR) in ^{16}O have not been well determined. Knöpfle *et al.* places 65–90% of the isoscalar energy weighted sum rule (EWSR) in the excitation energy range 16–27 MeV by inelastic α particle scattering from ^{16}O [6]. Random phase approximation (RPA) calculations performed by Krewald *et al.* [7] indicate an ISGQR near an excitation energy of 22 MeV (in agreement with Ref. [6]) and an isovector EWSR strength that is spread out above 30 MeV. This is in concurrence with Ref. [8], which provides evidence for $E2$ strength between 25 and 45 MeV excitation energy that exhausts approximately 68% of the isovector EWSR.

As with the present work, Mellendorf's [5] aim was to extract experimental parameters for an IVGQR in ^{16}O. Compton scattering cross sections were measured at 45 and 135° using unpolarized photons, and the $E2$ signature was investigated through the cross section ratio at these two angles. Mellendorf found no evidence for a compact IVGQR below E_γ=64 MeV. Instead it was speculated that approximately 50% of the isovector EWSR exists above 64 MeV.

This speculation disagrees with previous works mentioned above, as well as with systematics that are consistent with a semiclassical model that predicts the IVGQR excitation energy at $E_0^{E2}=57A^{-1/6}$ [9].

C. Present experiment

In order to investigate the goals outlined in Sec. I A, we have performed a Compton scattering experiment on ^{16}O using linearly polarized photons. The present work consisted of measurements of the polarization asymmetries $\Sigma(\theta_{\text{c.m.}})$ and $\Sigma(E_\gamma)$ at $E_\gamma=25$, 30, 35, 40 MeV and $\theta_{\text{c.m.}}=90$, 120, 135, 150°.

In this paper, we shall begin our discussion with a description of the details of the experiment. Next, our methods of data analysis will be relayed. Then, the polarization asymmetry results and their interpretation will be presented. Finally, conclusions based on the interpretation will be discussed.

II. EXPERIMENTAL DESCRIPTION

The present experiment was performed using the high-intensity, monochromatic beams of 100% linearly polarized γ rays produced at the High Intensity γ-ray Source (HI$\vec{\gamma}$S) situated in the Duke Free Electron Laser Laboratory (DFELL) at Duke University [10].

A. Photon beam parameters

The polarized γ rays are produced by Compton backscattering FEL photons from the DFELL storage ring electron beam [11]. The DFELL storage ring operated at energies between 600 and 760 MeV for the present HI$\vec{\gamma}$S experimental run. The resulting 4.8 eV FEL photons were scattered from electrons in the storage ring to produce 25–40 MeV γ rays. A 25.4 $\times$25.4 cm diameter NaI detector was placed in the beam at the rear of the experimental room for beam tuning purposes. This in-beam detector was energy calibrated by placing an Am-Be source approximately two meters from the face. The 4.43 MeV γ ray from the source along with the 6.8 MeV line corresponding to neutron capture on iodine in the NaI detector were used as the calibration points. To prevent saturation (and possible damage to components) of the detector, it was only turned on at times of low γ-ray fluxes. This detector was recalibrated on a daily basis with the Am-Be source and was used to determine the incident γ-ray energy and energy spread (typically $\Delta E/E\approx 10\%$). In addition, the in-beam NaI was used to calibrate a flux monitor paddle located just behind the front wall of the experimental room. This paddle is a thin plastic scintillator counter that is used to measure the incident flux at high photon rates. Using the flux monitor paddle calibrated with a "low" incident flux of $\sim 10^3\gamma$/s, the measured average flux was $(5\pm1)\times 10^5\gamma$/s on target through a 2.54 cm diameter lead collimator. The large error comes from extrapolating the low γ-ray flux paddle calibration to a region where the flux is 2 orders of magnitude higher. This error in γ-ray flux does not affect the uncertainty in the measured asymmetry.

B. Target and detectors

The target for this experiment consisted of a 25.4 cm long, 2.86 cm diameter thin-walled plastic cylinder filled with distilled water. Scattered γ rays from the target were detected by four unshielded 25.4 $\times$25.4 cm NaI detectors placed at azimuthal angles of 0, 90, 180, and 270°. These detectors were mounted on a supporting apparatus named the Eggbeater. The Eggbeater can place any single detector at any polar angle θ between 30 and 150° and any azimuthal angle ϕ between 0 and 360°. Both the Eggbeater and the target were aligned to the optical axis of the FEL with the help of a He-Ne alignment laser beam reflected down the axis. Before data acquisition began, the alignment relative to the γ-ray beam axis of the He-Ne laser was checked by placing an x-ray film directly in the γ-ray beam and observing the developed image. The laser alignment was found to be accurate to within ± 2 mm. The four NaI detectors on the Eggbeater were energy calibrated in the same manner as the in-beam NaI detector (i.e., using the Am-Be source).

C. Background reduction

Since the detected cosmic-ray and room background rates were determined to be comparable to the reaction count rate, a new background reduction technique was utilized. An operational mode of the FEL that produces so-called giant high peak power pulses (GHPP) [12] was employed to reduce cosmic-ray and room background by a factor of 100. By taking data only during the GHPP duration, 99% of the cosmic-ray and room background events, determined by the ratio of pulse width to pulse separation, can be eliminated. An additional reduction factor of 18 was obtained by use of a time-of-flight (TOF) cut generated from the natural time structure of the γ-ray beam. A more detailed description of this technique can be found in Ref. [13].

III. DATA ANALYSIS

A. Data reduction

Two basic types of spectra were obtained during the experiment, TOF and energy spectra. A typical TOF spectrum is shown in Fig. 1. The peak coming at earlier times is attributed to atomic Compton scattering events from the upstream collimator. The peak coming at later times corresponds to nuclear Compton scattering from the ^{16}O nuclei inside the H_2O target. As a check, it was verified that this right-hand peak vanished when the water target was replaced with an empty cell. The difference in timing between the two peaks was due to the net difference between the collimator-detector distance and the collimator-target-detector distance.

Placing a software cut around the nuclear Compton scattering timing peak resulted in an enhancement of the higher energy part of the energy spectrum. This enhancement was at energies consistent with those expected from nuclear Compton scattering from ^{16}O. One such energy spectrum is shown in Fig. 2. Since the energy spread in the beam dominated the total response function, a response function obtained by a direct in-beam measurement with a reduced beam intensity was used to fit the peak in each spectrum. The fitting routine

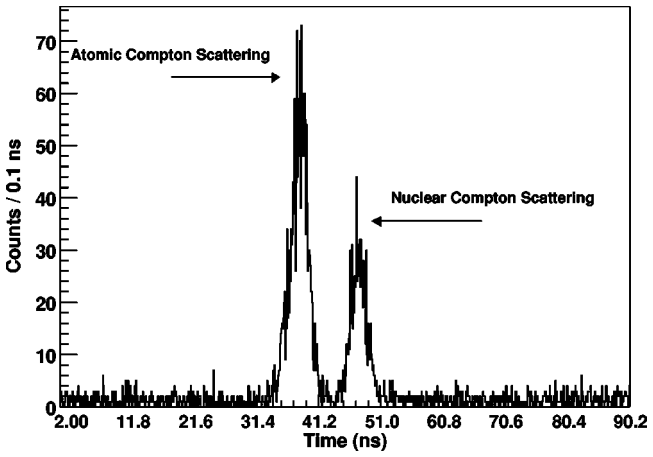

FIG. 1. A time-of-flight (TOF) spectrum with GHPP enabled. The detector was placed at $\theta_{lab}=135^{\circ}$.

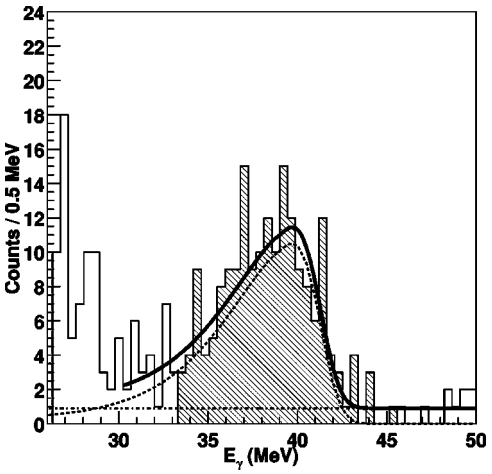

FIG. 2. An energy spectrum subject to a TOF cut and with GHPP enabled. The incident γ-ray energy was $E_\gamma=40$ MeV. The solid curve is the total fit, while the two dashed curves are the peak and background components. The shaded area indicates the summing region.

allowed the height, width, and centroid of the peak to be varied, but used the measured NaI response function to specify the shape of the distribution. Fitting the spectra allowed the centroid and width parameters to be extracted from each spectrum in a consistent manner. The actual data were summed over a region defined by the fit parameters. In particular, each energy histogram was summed from two full widths at half maximum (FWHMs) below the centroid to one FWHM above. In Fig. 2, the summing region is indicated by the shaded area. The cosmic-ray background was subtracted by fitting the portion of the energy spectrum above the peak with a horizontal line, and the integral of this background fit, normalized to the same number of channels, was subtracted from the peak histogram sum. These background-subtracted sums comprised the set of detector yields used in determining the experimental asymmetries.

B. Experimental asymmetry

The experimental asymmetry is given by

$$\Sigma = \frac{N_{\parallel} - N_{\perp}}{N_{\parallel} + N_{\perp}},$$

which can also be written in the case of four detectors in two orientations as

$$\Sigma = \frac{1 - R}{1 + R}, \tag{1}$$

where R is a ratio combining two different orientations of the Eggbeater:

$$R = \sqrt{\frac{N_{\perp A} N_{\perp B}}{N_{\parallel A} N_{\parallel B}}}. \tag{2}$$

The $\perp$ and $\parallel$ subscripts denote detector yields perpendicular and parallel to the polarization plane of the incident γ ray, respectively. Likewise, the A and B subscripts denote the initial orientation of the detectors and the orientation of the detectors rotated by 90° in ϕ with respect to the initial orientation, respectively. Periodically, during data taking, the Eggbeater was rotated by 90° in ϕ from orientation A to B. The quantity $N_{\perp A}$ ($N_{\parallel A}$) is the sum of the yields of the two detectors placed in the plane perpendicular (parallel) to the polarization plane of the incident γ rays for orientation A. An identical description pertains to $N_{\perp B}$ ($N_{\parallel B}$).

Using the ratio R [Eq. (2)] formed from these two orientations, one can eliminate uncertainties due to the absolute γ-ray flux measurement and systematic differences in the detectors from the calculation of the asymmetry Σ [Eq. (1)]. For example, the two detectors that were used to generate the yield $N_{\perp A}$ are the same detectors that correspond to the yield $N_{\parallel B}$ once the Eggbeater is rotated by $\phi=90°$. So, the effective efficiency of these two detectors cancels out of the ratio R. As mentioned in Sec. II A, the absolute γ-ray flux cancels out of the ratio since it is a common factor for both $N_{\perp A}$ and $N_{\parallel A}$.

C. Conventional formalism for compton scattering

The theoretical formalism used for calculating the Compton scattering cross section as a function of photon energy and polarization scattering angle follows that of Ref. [14]. The key equations are presented here. The elastic differential cross section is written as the square of the modulus of a complex scattering amplitude:

$$\frac{d\sigma}{d\Omega}(E,\theta) = |R(E,\theta,\phi)|^2. \tag{3}$$

The scattering amplitude has the form

$$R(E,\theta,\phi) = \sum_{\lambda} f^{\lambda}(E) g_{\lambda}(\theta,\phi) + D(E,\theta,\phi), \tag{4}$$

where

$$f^{\lambda}(E) = \mathrm{Re}[f^{\lambda}(E)] + i\ \mathrm{Im}[f^{\lambda}(E)] \tag{5}$$

and

TABLE I. Nucleon density parameters for determining the form factors $F_j(q)$. The values for $j=1$ are taken from Ref. [17]. Varying c_2 effectively alters the average charge radius of $F_2(q)$ [4].

j	c_j (fm)	w_j	z_j (fm)
1	2.608	−0.051	0.513
2	0.888−1.674	−0.051	0.513

$$\lambda = E1, M1, E2, \ldots .$$

The $f^{\lambda}(E)$ are complex forward scattering amplitudes for scattering from the internal degrees of freedom of the nucleus for a particular multipole λ, and the $g_{\lambda}(\theta)$ are angular factors for a specific multipole λ. $D(E,\theta)$ is called the modified Thomson amplitude.

The forward scattering amplitudes are related to the total photoabsorption cross section $\sigma_{\gamma}(E)$ by

$$\mathrm{Im}[f^{\lambda}(E)] = \frac{E}{4\pi\hbar c}\sigma_{\gamma}^{\lambda}(E) \tag{6}$$

and

$$\mathrm{Re}[f^{\lambda}(E)] = \frac{E^2}{2\pi^2\hbar c}\int_0^{m_{\pi}c^2} \frac{\sigma_{\gamma}^{\lambda}(E')}{E'^2 - E^2}dE', \tag{7}$$

with

$$\sigma_{\gamma}(E) = \sum_{\lambda} \sigma_{\gamma}^{\lambda}(E). \tag{8}$$

Equation (6) is the optical theorem applied to each multipole separately, and Eq. (7) is a once-subtracted dispersion relation.

The modified Thomson amplitude is written as

$$\begin{aligned} D(E,\theta,\phi) = &- Zr_0F_1(q)g_{E1}(\theta,\phi) \\ &+ AF_1(q)\left(\frac{E}{\hbar c}\right)^2[\overline{\alpha}g_{E1}(\theta,\phi) + \overline{\beta}g_{M1}(\theta,\phi)] \\ &+ \frac{NZ}{A}r_0g_{E1}(\theta,\phi)\{1 + \kappa[1 - F_2(q)]\}, \end{aligned} \tag{9}$$

where $r_0 = e^2/M_pc^2$ is the classical radius of the proton, $\overline{\alpha}$ and $\overline{\beta}$ are the nucleon polarizabilities, and κ is an enhancement factor due to meson exchange. For ^{16}O, κ has been measured to be 0.95 [15]. The one-body form factor $F_1(q)$ and two-body form factor $F_2(q)$ can both be written in the form [5]

$$F_j(q) = \int \rho_j(\vec{r})e^{i\vec{q}\cdot\vec{r}}d^3r, \quad j = 1,2$$

with the nucleon density for each modeled by the three-parameter Fermi function

$$\rho_j(r) = \frac{1 + w_jr^2/c_j^2}{1 + \exp[(r - c_j)/z_j]}, \tag{10}$$

where the values of the parameters c_j, w_j, and z_j are given in Table I.

TABLE II. Lorentzian parameterization for the total photoabsorption cross section $\sigma_{\gamma}(E)$.

E_0 (MeV)	Γ_0 (MeV)	σ_0 (mb)
13.12	1.12	5.79
17.20	0.44	4.54
20.92	0.57	4.87
22.23	0.71	26.52
23.01	0.23	15.79
24.26	0.28	11.83
24.70	5.17	18.09
33.03	14.25	2.86

Using the formalism described in this section, the asymmetry is constructed

$$\Sigma(E,\theta) = \frac{1 - (d\sigma/d\Omega)_{\perp}/(d\sigma/d\Omega)_{\parallel}}{1 + (d\sigma/d\Omega)_{\perp}/(d\sigma d\Omega)_{\parallel}}, \tag{11}$$

where

$$\frac{d\sigma}{d\Omega}_{\perp}(E,\theta) = |R_{\perp}(E,\theta)|^2$$

and

$$\frac{d\sigma}{d\Omega}_{\parallel}(E,\theta) = |R_{\parallel}(E,\theta)|^2.$$

D. Parameters used in calculations

It is convenient to represent the total photoabsorption cross section $\sigma_{\gamma}(E)$ as a sum of Lorentzian line shapes [16]. Since the present HI$\vec{\gamma}$S data will be combined with the data taken by Mellendorf [4,5], the parametrization chosen was identical to that contained in Ref. [5]. The values used, which give a good description of the experimental data, are shown in Table II. The values for $g_{\lambda}(\theta)$ are presented in Table III [14].

The parametrization of the two-body nucleon density $\rho_2(r)$ is not unique. The form factor $F_2(q)$ is poorly known. Adjusting the parameter c_2 effectively varies the mean square radius of the distribution. This parameter was varied from 0.888 to 1.674 to investigate the sensitivity of $\Sigma(E,\theta)$ [Eq. (11)] to the two-body form factor $F_2(q)$. No difference was seen in the calculated curves within the energy range of the present experiment.

TABLE III. Angular factors for scattering amplitudes. λ denotes the multipolarity. $(\hat{k},\hat{\epsilon})$ and $(\hat{k}',\hat{\epsilon}')$ are the direction and polarization of the incident and scattered photons, respectively.

λ	$g_{\lambda}(\theta,\phi)$	$g_{\lambda\parallel}(\theta)$	$g_{\lambda\perp}(\theta)$
E1	$\epsilon\cdot\epsilon'$	$\cos(\theta)$	1
M1	$(\hat{\epsilon}\times\hat{k})\cdot(\hat{\epsilon}'\times\hat{k}')$	1	$\cos(\theta)$
E2	$(\hat{\epsilon}\cdot\hat{\epsilon}')(\hat{k}\cdot\hat{k}')+(\hat{\epsilon}\cdot\hat{k}')(\hat{\epsilon}'\cdot\hat{k})$	$2\cos^2(\theta)-1$	$\cos(\theta)$

Whether or not the in-medium nucleon polarizabilities of ^{16}O are the same as the corresponding free nucleon values is debatable [3,4]. Conventionally, the sum of the polarizabilities $\bar{\alpha}+\bar{\beta}$ is constrained by the Baldin sum rule to be 14.2 $\times 10^{-4}$ fm^3 [18], but the difference $\bar{\alpha}-\bar{\beta}$ is not well known. Reference [4] includes additional terms (proportional to E^2) in the modified Thomson amplitude, which correspond to a two-body exchange contribution. These terms are identical in form to the second term in Eq. (9) with $F_1(q)$, $\bar{\alpha}$, and $\bar{\beta}$ replaced by $F_2(q)$, $\bar{\alpha}_{ex}$, and $\bar{\beta}_{ex}$, respectively. Nonzero values of $\bar{\alpha}_{ex}$ and $\bar{\beta}_{ex}$ (which formally look like polarizabilities, but are treated as phenomenological parameters) give the energy dependence to the two-body portion of the scattering amplitude mentioned in Sec. I A. The inclusion of these parameters leads to a sum rule similar to the Baldin sum rule that says $\bar{\alpha}+\bar{\beta}+\bar{\alpha}_{ex}+\bar{\beta}_{ex}\approx 15\times 10^{-4}$ fm^3 [4]. This sum rule constraint will be used in the present analysis, and we take the free values of the nucleon polarizabilities as $\bar{\alpha}=11.5$ $\times 10^{-4}$ fm^3 and $\bar{\beta}=3.5\times 10^{-4}$ fm^3. To investigate the sensitivity of the present data to modifications of the free values of the nucleon polarizabilities and to a significant energy dependence of the two-body scattering amplitude, the same values of the deviations as in Ref. [4] will be used. These are $\Delta\bar{\beta}=-\Delta\bar{\alpha}=8$, $\bar{\beta}_{ex}=-\bar{\alpha}_{ex}=0$ (designated as Modification I), and $\Delta\bar{\beta}=-\Delta\bar{\alpha}=0$, $\bar{\beta}_{ex}=-\bar{\alpha}_{ex}=5$ (designated as Modification II) , where Δ refers to the change relative to the free value.

IV. ASYMMETRY RESULTS

A. Narrow IVGQR

The choice of the initial IVGQR excitation energy for ^{16}O was guided by the result of a semiclassical calculation by Suzuki [19], which predicts $E_0^{E2}=57A^{-1/6}$. This result has been shown to be close to experimental results in the light nuclei [9]. The $A^{-1/6}$ dependence comes from large contributions of surface effects to the restoring force of the resonance. A reasonably narrow resonance width ($\Gamma_0^{E2}=6$ MeV) was chosen consistent with systematic studies of other nuclei.

The present HI$\vec{\gamma}$S data and data from Refs. [3–5] are shown in Figs. 3–5. The error bars on the present data represent the statistical uncertainties associated with the data points. The solid curves are a prediction without the inclusion of an IVGQR. In other words, they are a prediction based purely on scattering through the high energy tail of the giant dipole resonance (GDR) in ^{16}O. Within error, the HI$\vec{\gamma}$S data follow the pure GDR curves. The dashed curves in Figs. 3(a), 4(a), and 5(a) are a prediction that includes an IVGQR with $E_0^{E2}=36$ MeV and $\Gamma_0^{E2}=6$ MeV, which exhausts 100% of the isovector EWSR. Both the dotted and the dot-dashed curves include the same IVGQR as well as Modification I and II, respectively.

Collectively, these data do not support the existence of a narrow IVGQR below 40 MeV. However, as will be shown below, a broad resonance below 40 MeV is not ruled out. This agrees with both the theory [7] and experiments [5,8] previously discussed.

B. Broad IVGQR with polarizability modifications

The experiment of Phillips *et al.* indicates that approximately 68% of the isovector EWSR is exhausted by an

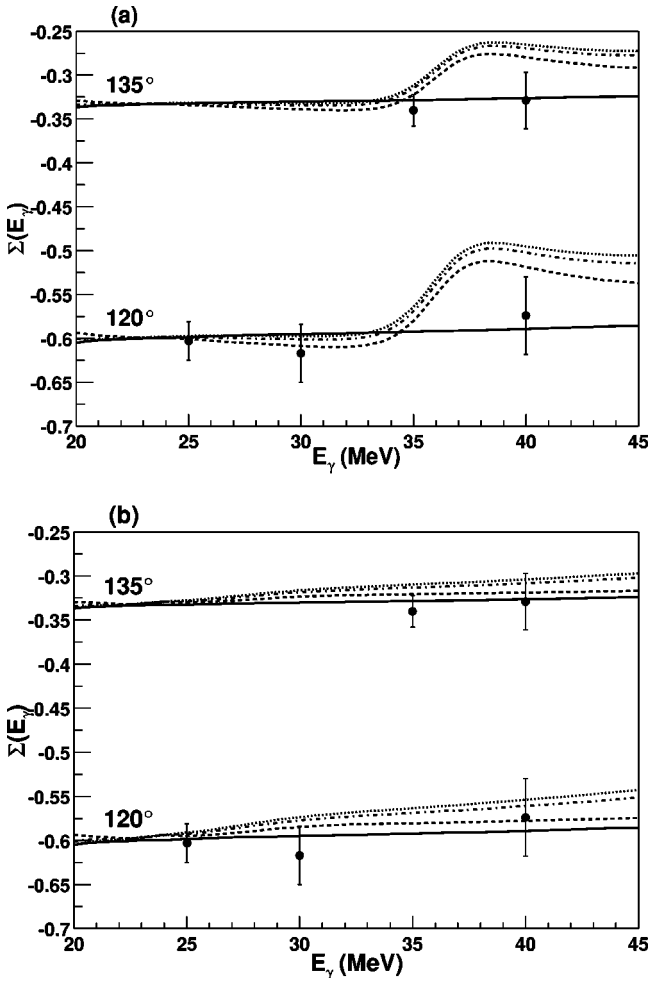

FIG. 3. Asymmetry as a function of incident γ-ray energy. The filled circles are the present HI$\vec{\gamma}$S data. The error bars are statistical only. The solid curves are pure GDR predictions. In (a), the dashed curve includes an IVGQR with parameters $E_0^{E2}=36$ MeV, $\Gamma_0^{E2}=6$ MeV, and 100% EWSR. In (b), the dashed curve includes an IVGQR with parameters $E_0^{E2}=28.3$ MeV, $\Gamma_0^{E2}=12.9$ MeV, and 68% EWSR. The dotted curves include the respective IVGQR and Modification I as discussed in the text. The dot-dashed curves include the respective IVGQR and Modification II.

IVGQR located between 25 and 45 MeV [8]. The E2 cross section data contained in this paper was fit by a single Lorentzian by the present authors to extract quantitative parameters for the IVGQR. The parameters obtained from the fit are $E_0^{E2}=28.3\pm 1.2$ MeV and $\Gamma_0^{E2}=12.9\pm 3.6$ MeV. The $E2$ resonance was scaled so that it exhausted 68% of the isovector EWSR.

Figures 3(b), 4(b), and 5(b) show again the three data sets as before, but now with the inclusion of a broad IVGQR instead of a narrow one. The solid curves are a prediction without the inclusion of an IVGQR. The dashed curves are a prediction that includes an IVGQR with $E_0^{E2}=28.3$ MeV and $\Gamma_0^{E2}=12.9$ MeV, which exhausts 68% of the isovector EWSR. Both the dotted and the dot-dashed curves include the same IVGQR as well as Modification I and II, respectively.

The HI$\vec{\gamma}$S data support the hypothesis that a broad IVGQR could be present below 40 MeV, but the uncertainty

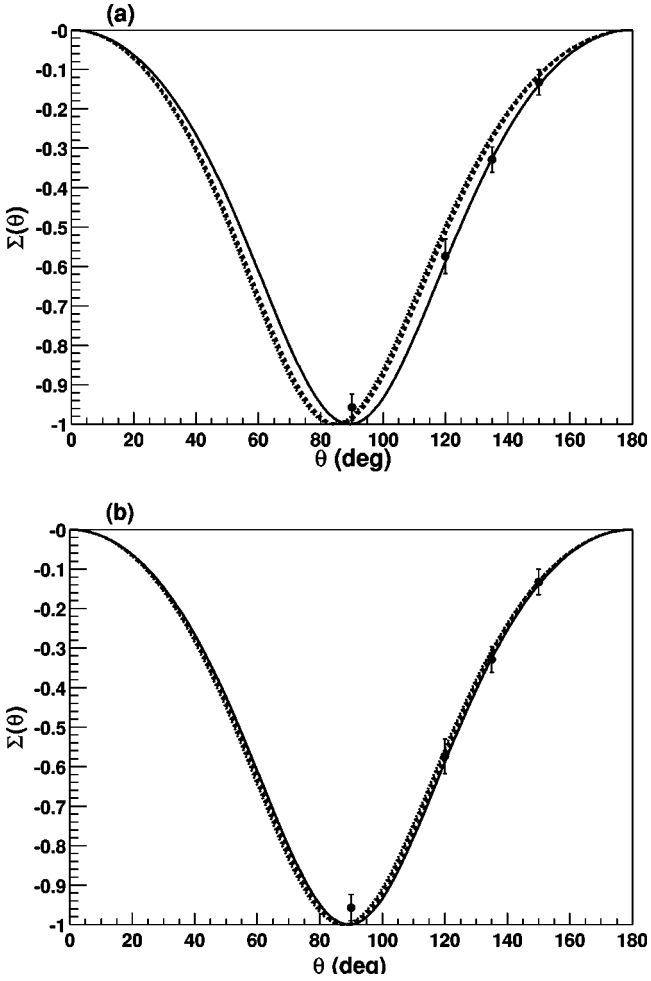

FIG. 4. Asymmetry as a function of scattering angle. The filled circles are the present HI$\vec{\gamma}$S data. The error bars are statistical only. See caption to Fig. 3 for definition of curves.

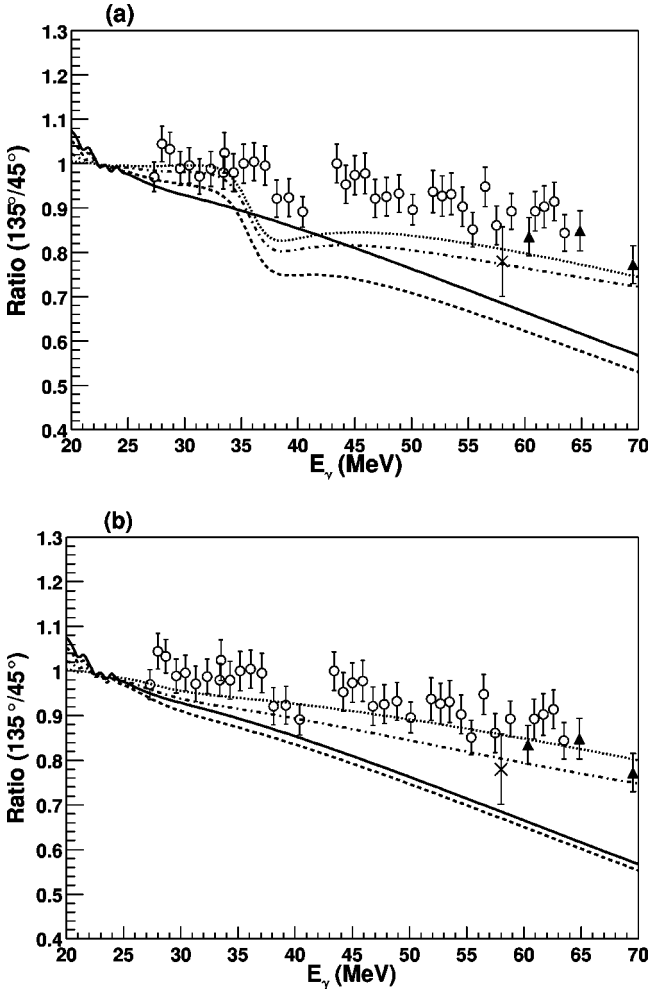

FIG. 5. Ratio of cross sections measured at 45° and 135°. The open circles and the triangles are from Ref. [4]. The X's are from Ref. [2]. See caption to Fig. 3 for definition of curves.

in the measurements is too great to definitely establish the existence of this state. The data in Fig. 5(b), once Modification I or II is applied, also cannot rule out large, broad $E2$ strength below 40 MeV.

As seen in Figs. 3 and 4, the HI$\vec{\gamma}$S data cannot distinguish between modifications of the free values of the nucleon polarizabilities (or equivalently, to the addition of a significant energy dependence of the two-body portion of the scattering amplitude). In other words, the present data do not alter the conclusions drawn in Ref. [4].

V. CONCLUSIONS

The first nuclear Compton scattering experiment performed at the HI$\vec{\gamma}$S facility has been completed. Measurements of the polarization asymmetries have been performed for the first time with polarized photons on ^{16}O, and the data analyzed. Combining the present data with results from previous (unpolarized) measurements yields the conclusion that no narrow IVGQR exists below 40 MeV. However, even though the data are consistent with a pure GDR picture, they do not rule out a broad $E2$ resonance between 25 and 45 MeV that exhausts a large percentage of the isovector EWSR. In addition, the HI$\vec{\gamma}$S data do not rule out the possibility of modifications of the nucleon polarizabilities in accord with Ref. [4]. The present work reinforces the conclusions of previous works.

These results demonstrate the potential of the HI$\vec{\gamma}$S facility for performing precision measurements of analyzing powers in Compton scattering. Since the uncertainties in the measured asymmetries are dominated by statistics, the anticipated increase in beam intensities by at least two orders of magnitude should provide precision results. This increase is a part of the present HI$\vec{\gamma}$S upgrade project, which should be completed by late 2006. A detailed program of Compton scattering measurements on polarized and unpolarized targets of protons, deuterons, ^{3}He, and ^{4}He (unpolarized) is being developed.

ACKNOWLEDGMENTS

We thank the technical personnel and the operations group of the DFELL for providing excellent γ-ray beams. We thank Dr. Al Nathan for useful discussions regarding the interpretation of the results. This work was supported by the AFOSR under Grant No. F49620-00-10370 and by the U.S.-DOE under Grant No. DE-FG02-97ER-41033, No. DE-FG02-91ER-40609, and No. DE-FG02-91ER-41046.

[1] D. S. Dale, R. M. Laszewski, and R. Alarcon, Phys. Rev. Lett. **68**, 3507 (1992).
[2] D. Häger *et al.*, Nucl. Phys. **A595**, 287 (1995).
[3] M.-T. Hüit, A. I. L'vov, A. I. Milstein, and M. Shumacher, Phys. Rep. **323**, 457 (2000).
[4] G. Feldman *et al.*, Phys. Rev. C **54**, R2124 (1996).
[5] K. E. Mellendorf, Ph.D. thesis, Univ. of Illinois (1993) (University Microfilms International).
[6] K. T. Knöpfle, G. J. Wagner, H. Breur, M. Rogge, and C. Mayer-Böricke, Phys. Rev. Lett. **35**, 779 (1975).
[7] S. Krewald, J. Birkholz, Amand Faessler, and J. Speth, Phys. Rev. Lett. **33**, 1386 (1974).
[8] T. W. Phillips and R. G. Johnson, Phys. Rev. C **20**, 1689 (1979).
[9] S. Ito *et al.*, in *Proceedings of the IV International Symposium on Weak and Electromagnetic Interactions in Nuclei*, Osaka (World Scientific, Singapore, 1995), pp. 455–458.
[10] H. R. Weller and M. W. Ahmed, Mod. Phys. Lett. A **18**, 1569 (2003).
[11] V. N. Litvinenko *et al.*, Nucl. Instrum. Methods Phys. Res. A **407** 8 (1998).
[12] I. V. Pinayev, V. N. Litvinenko, S. H. Park, Y. Wu, M. Emamian, N. Hower, J. Patterson, and G. Swift, Nucl. Instrum. Methods Phys. Res. A **475**, 222 (2001).
[13] M. W. Ahmed *et al.*, Nucl. Instrum. Methods Phys. Res. A **516**, 440 (2004).
[14] D. H. Wright, P. T. Debevec, L. J. Morford, and A. M. Nathan, Phys. Rev. C **32**, 1174 (1985).
[15] J. Ahrens *et al.*, Nucl. Phys. **A251**, 479 (1975).
[16] S. F. LeBrun, A. M. Nathan, and S. D. Hoblit, Phys. Rev. C **35**, 2005 (1987).
[17] C. W. De Jager *et al.*, At. Data Nucl. Data Tables **14**, 479 (1974).
[18] A. M. Baldin, Nucl. Phys. **18**, 310 (1960).
[19] T. Suzuki, Prog. Theor. Phys. **64**, 1627 (1980).